Transverse-momentum resummation for gauge boson pair production at the hadron collider

Yan Wang,[1] Chong Sheng Li,[1,2,*] Ze Long Liu,[1] Ding Yu Shao,[1] and Hai Tao Li[1]

[1]*Department of Physics and State Key Laboratory of Nuclear Physics and Technology, Peking University, Beijing 100871, China*
[2]*Center for High Energy Physics, Peking University, Beijing 100871, China*

(Received 11 August 2013; published 4 December 2013)

We perform the transverse-momentum resummation for W^+W^-, ZZ, and $W^\pm Z$ pair productions at the next-to-next-to-leading logarithmic accuracy using soft-collinear effective theory for $\sqrt{S} = 8$ TeV and $\sqrt{S} = 14$ TeV at the LHC, respectively. Importantly, this is the first calculation of $W^\pm Z$ transverse-momentum resummation. We also include the nonperturbative effects and discussions on the PDF uncertainties. Comparing with the next-to-leading logarithmic results, the next-to-next-to-leading logarithmic resummation can reduce the dependence of the transverse-momentum distribution on the factorization scales significantly. Finally, we find that our numerical results are consistent with data measured by the CMS Collaboration for the ZZ production, which have thus far only been reported by the LHC experiments for the unfolded transverse-momentum distribution of the gauge boson pair production within theoretical and experimental uncertainties.

DOI: 10.1103/PhysRevD.88.114017 PACS numbers: 14.65.Ha, 12.38.Bx, 12.60.Fr

I. INTRODUCTION

The gauge boson pair productions are important within and beyond the Standard Model (SM). For the cases of W^+W^- and $W^\pm Z$ productions, they can be used to test the non-Abelian gauge structure, especially triple-gauge-boson couplings. Besides, W^+W^- and ZZ are irreducible SM backgrounds of Higgs boson production. If there is any deviation from the predictions of SM, it may be a new physics signal. Therefore, it is essential to count on accurate theoretical predictions for these processes.

Experimental collaborations at the Tevatron and the LHC have reported experimental results of various kinematic distributions for W^+W^-, ZZ, $W^\pm Z$ productions. The leptonic decay mode of the gauge boson pair has been analyzed at the Tevatron [1–5] and at the LHC for $\sqrt{S} = 7$ and $\sqrt{S} = 8$ TeV, respectively [6,7]. In addition, more stringent limitations on anomalous triple-gauge-boson couplings, compared with those of the past, have been presented by the LHC Collaboration [8–10].

Furthermore, if the gauge boson pair comes from the decay of a heavy resonance, the kinematics of the gauge boson pair will carry information of the resonance. Therefore, it is necessary to consider the boson pair as a unit, rather than consider each individual gauge boson. The transverse-momentum q_T of the boson pair system is one important observable, which has been measured at the LHC [9,11,12].

The next-to-leading order (NLO) QCD corrections to W^+W^-, ZZ, and $W^\pm Z$ production were calculated many years ago [13–17]. Besides, NLO QCD corrections with the helicity amplitudes method were completed in Ref. [18], where the effects of spin correlation were fully taken into account. Recently, two-loop virtual QCD corrections to W^+W^- production in the high-energy limit have been reported in Ref. [19], and threshold resummation in the soft-collinear effective theory (SCET) and the approximate NNLO cross sections for W^+W^- production are calculated in Ref. [20]. $W^\pm Z$ production is calculated beyond NLO QCD for high q_T region [21]. However, when the invariant mass of gauge boson pair M is much larger than q_T, there exist large logarithmic terms of the form $\ln(q_T^2/M^2)$ in the small q_T region. The fixed-order predictions are invalid in this region. Therefore it is necessary to resum these large logarithmic terms to all order.

In this paper, we calculate the transverse-momentum resummation of the gauge boson pair production at the next-to-next-to-leading logarithmic (NNLL) accuracy based on SCET [22–24]. In the case of transverse-momentum resummation, frameworks equivalent to the Collins, Soper, and Sterman (CSS) formalism have been developed for both the Drell-Yan process and Higgs production [25–33]. The framework we adopted in the paper is built upon Refs. [32,33]. In the case of W^+W^- and ZZ pair production, q_T resummation has been discussed in the CSS framework [34–36]. However, to our knowledge, the resummation effects on the transverse momentum of $W^\pm Z$ production have not been calculated so far.

The paper is organized as follows. In Sec. II, we describe the formalism for q_T resummation in SCET briefly. In Sec. III, we present our numerical results. Section IV is a brief conclusion.

II. FACTORIZATION AND RESUMMATION

In this section, we briefly review the transverse-momentum resummation in SCET formalism in Refs. [32,33]. The resummation formulas of transverse-momentum distribution we used can be applied to the processes where nonstrongly interacting particles are produced in hadronic collisions.

*csli@pku.edu.cn

We consider the processes

$$N_1(P_1) + N_2(P_2) \to V_l(p_3) + V_m(p_4) + X(p_x), \quad (1)$$

where $V_{l,m}$ (l, $m = W$, Z) is W or Z boson, and X is an inclusive hadronic final state. In the Born level, the partonic process is

$$q(p_1) + q'(p_2) \to V_l(p_3) + V_m(p_4), \quad (2)$$

where $p_i = z_i P_i$, $i = 1, 2$. The kinematic variables are defined as follows:

$$S = (P_1 + P_2)^2, \quad s = (p_1 + p_2)^2, \quad t = (p_1 - p_3)^2,$$
$$u = (p_2 - p_3)^2, \quad q = p_3 + p_4, \quad q^2 = M^2,$$
$$\tau = (M^2 + q_T^2)/S. \quad (3)$$

In the kinematical region of $\Lambda^2_{\rm QCD} \ll q_T^2 \ll M^2$, soft and collinear emissions can be treated in the SCET framework. After performing the phase space integration over the individual gauge boson, we obtain the factorized differential cross section as [37]

$$\frac{d^3\sigma}{dq_T^2 dy dM^2} = \frac{1}{S}\mathcal{H}_{V_lV_m}(M, \mu_f)\frac{1}{4\pi}\int d^2x_\perp e^{-iq_\perp\cdot x_\perp} \times \sum_{q,q'}[\mathcal{B}_{q/N_1}(z_1, x_T^2, \mu_f)\mathcal{B}_{q'/N_2}(z_2, x_T^2, \mu_f) + (q \leftrightarrow q')], \quad (4)$$

where y is the rapidity of the boson pair system, μ_f is the factorization scale, and $z_{1,2} = \sqrt{\tau}e^{\pm y}$. Here $\mathcal{H}_{V_lV_m}$ is the hard function and can be expanded as

$$\mathcal{H}_{V_lV_m} = \mathcal{H}^{(0)}_{V_lV_m} + \frac{\alpha_s}{4\pi}\mathcal{H}^{(1)}_{V_lV_m} + \cdots. \quad (5)$$

As a cross-check, we recalculate $\mathcal{H}^{(0)}_{V_lV_m}$ and $\mathcal{H}^{(1)}_{V_lV_m}$ and find that our results are consistent with those in Refs. [13,14,38], and the corresponding details are listed in Appendix A. The renormalization-group (RG) equation of hard function can be written as

$$\frac{d}{d\ln\mu}\mathcal{H}_{V_lV_m}(M, \mu) = 2\left[\Gamma^F_{\rm cusp}(\alpha_s)\ln\frac{-M^2}{\mu^2} + 2\gamma^q(\alpha_s)\right]\mathcal{H}_{V_lV_m}(M, \mu), \quad (6)$$

where $\Gamma^F_{\rm cusp}(\alpha_s)$ is the cusp anomalous dimension of Wilson loops with lightlike segments, while $\gamma^q(\alpha_s)$ controls the single-logarithmic evolution. After solving the RG equation, we obtain the hard function

$$\mathcal{H}_{V_lV_m}(M, \mu_f) = \exp\left[4S(\mu_h^2, \mu_f^2) - 2a_\Gamma(\mu_h^2, \mu_f^2)\ln\frac{-M^2}{\mu_h^2} - 4a_{\gamma^q}(\mu_h^2, \mu_f^2)\right]\mathcal{H}_{V_lV_m}(M, \mu_h), \quad (7)$$

where μ_h is the hard matching scale. Here $S(\nu^2, \mu^2)$ and $a_\Gamma(\nu^2, \mu^2)$ are defined as

$$S(\nu^2, \mu^2) = -\int_{\alpha_s(\nu^2)}^{\alpha_s(\mu^2)} d\alpha \frac{\Gamma^F_{\rm cusp}(\alpha)}{\beta(\alpha)}\int_{\alpha_s(\nu^2)}^{\alpha}\frac{d\alpha'}{\beta(\alpha')}, \quad (8)$$

$$a_\Gamma(\nu^2, \mu^2) = -\int_{\alpha_s(\nu^2)}^{\alpha_s(\mu^2)} d\alpha \frac{\Gamma^F_{\rm cusp}(\alpha)}{\beta(\alpha)}. \quad (9)$$

a_{γ^q} has a similar expression. Up to NNLL level, we need a three-loop cusp anomalous dimension and a two-loop normal anomalous dimension, and their explicit expressions are collected in the Appendixes of Ref. [39].

In the hard function, there will be large π^2 terms when we choose the hard scale as $\mu_h^2 \sim M^2$, which will spoil the perturbative convergence. The poor perturbative behavior can be avoid if we evaluate the hard function at the timelike region $\mu_h^2 \sim -M^2$, by applying the solution of RG in Eq. (6) to evolve μ_h^2 from the spacelike region to timelike region. As a result, π^2-enhanced terms can be resummed to all orders [40].

The function $\mathcal{B}_{q/N}$ in Eq. (4) is the transverse-momentum-dependent PDFs, which is defined by operator product expansion [32]. We adopt the analytic regularization of Ref. [41], and the product of the two $\mathcal{B}_{q/N}$ can be refactorized as

$$[\mathcal{B}_{q/N_1}(z_1, x_T^2, \mu_f)\mathcal{B}_{q'/N_2}(z_2, x_T^2, \mu_f)]_{q^2} = \left(\frac{x_T^2 q^2}{4e^{-2\gamma_E}}\right)^{-F_{qq'}(x_T^2, \mu_f)} B_{q/N_1}(z_1, x_T^2, \mu_f)B_{q'/N_2}(z_2, x_T^2, \mu_f), \quad (10)$$

where $F_{qq'}$ controls hidden q^2 dependence induced by collinear anomaly [32] and $B_{q/N}(z, x_T^2, \mu_f)$ can be matched onto the standard PDF via

$$B_{q/N}(z, x_T^2, \mu_f) = \sum_i \int I_{q\leftarrow i}(\xi, x_T^2, \mu_f)\phi_{i/N}(z/\xi, \mu_f)\frac{d\xi}{\xi} + \mathcal{O}(\Lambda^2_{\rm QCD}x_T^2), \quad (11)$$

where $x_T \ll \Lambda^{-1}_{\rm QCD}$ and $I_{q\leftarrow i}(z, x_T^2, \mu_f)$ are the matching coefficient functions [33]. The RG equations for the matching coefficient $I_{q\leftarrow i}(z, x_T^2, \mu_f)$ are given by

$$\frac{d}{d\ln\mu}I_{q\leftarrow i}(z, x_T^2, \mu) = [\Gamma^F_{\rm cusp}(\alpha_s)L_\perp - 2\gamma^q(\alpha_s)]I_{q\leftarrow i}(z, x_T^2, \mu) - \sum_j\int_z^1\frac{du}{u}I_{q\leftarrow j}(u, x_T^2, \mu)\mathcal{P}_{j\leftarrow i}(z/u, \alpha_s), \quad (12)$$

where $\mathcal{P}_{j\leftarrow i}$ is the Dokshitzer-Gribov-Lipatov-Altarelli-Parisi (DGLAP) splitting function and $L_\perp$ is defined as

$$L_\perp = \ln\frac{x_T^2\mu^2}{4e^{-2\gamma_E}}. \quad (13)$$

After factoring out the double logarithmic terms in $I_{q\leftarrow j}(z, x_T^2, \mu_f)$ we have

$$I_{q\leftarrow j}(z, x_T^2, \mu_f) \equiv e^{h_F(L_\perp, \alpha_s)} \bar{I}_{q\leftarrow j}(z, L_\perp, \alpha_s), \quad (14)$$

where $\bar{I}_{q\leftarrow j}$ satisfies as a DGLAP equation with an opposite sign [33], and the RG equation for $h_F(L_\perp, \alpha_s)$ is

$$\frac{d}{d\ln\mu} h_F(L_\perp, \alpha_s) = \Gamma^F_{\rm cusp}(\alpha_s) L_\perp - 2\gamma^q(\alpha_s). \quad (15)$$

After combining the above results, we can get the factorized cross section

$$\begin{aligned}\frac{d^2\sigma}{dq_T^2 dy} = \frac{1}{S} \sum_{i,j=q,q',g} \mathcal{H}_{VV}(M, \mu_f) \int_{\xi_1}^1 \frac{dz_1}{z_1} \int_{\xi_2}^1 \frac{dz_2}{z_2} \\ \times \bar{C}_{qq'\to ij}(z_1, z_2, q_T^2, \mu_f) \\ \times [\phi_{i/N_1}(\xi_1/z_1, \mu_f)\phi_{j/N_2}(\xi_2/z_2, \mu_f) \\ + (q, i \leftrightarrow q', j)]. \end{aligned} \quad (16)$$

Here $\bar{C}_{qq'\to ij}$ is the hard kernel of the process and defined as

$$\begin{aligned}&\bar{C}_{qq'\to ij}(z_1, z_2, q_T^2, \mu_f) \\ &= \frac{1}{2} \int_0^\infty dx_T x_T J_0(x_T q_T) \exp[g_F(\eta, L_\perp, \alpha_s)] \\ &\times [\bar{I}_{q\leftarrow i}(z_1, L_\perp, \alpha_s) \bar{I}_{q'\leftarrow j}(z_2, L_\perp, \alpha_s)], \end{aligned} \quad (17)$$

where J_0 is the zeroth-order Bessel function, and $g_F(\eta, L_\perp, \alpha_s)$ combines all the exponent terms [33], with $\eta \equiv \Gamma_0^F \alpha_s \ln\frac{M^2}{\mu^2}$. In order to avoid a factorially divergent term, we use the modified power-counting scheme and expand formulas with an auxiliary parameter ϵ, where $\alpha_s \sim \epsilon$ and $L_\perp \sim \epsilon^{-1/2}$. The expression for g_F can be found in Ref. [33].

In addition to singular terms, which are resummed by Eq. (16), fixed-order computation also contributes nonsingular terms to the total cross section. We need to combine the resummation result and the fixed-order result together for the q_T spectrum. Finally, in order to avoid double counting, the RG improved predictions for the transverse momentum of the gauge boson pair can be written as [33]

$$\begin{aligned}\frac{d\sigma^{\rm NNLL+NLO}}{dq_T} = \frac{d\sigma^{\rm NNLL}}{dq_T} \\ + \left[\frac{d\sigma^{\rm NLO}}{dq_T} - \frac{d\sigma^{\rm NNLL}}{dq_T}\right]_{\text{expanded to NLO}}. \end{aligned} \quad (18)$$

III. NUMERICAL RESULTS

In this section, we present the numerical results for the transverse-momentum resummation effects on gauge boson pair productions at the LHC. Unless specified otherwise, we choose SM input parameters as [42]

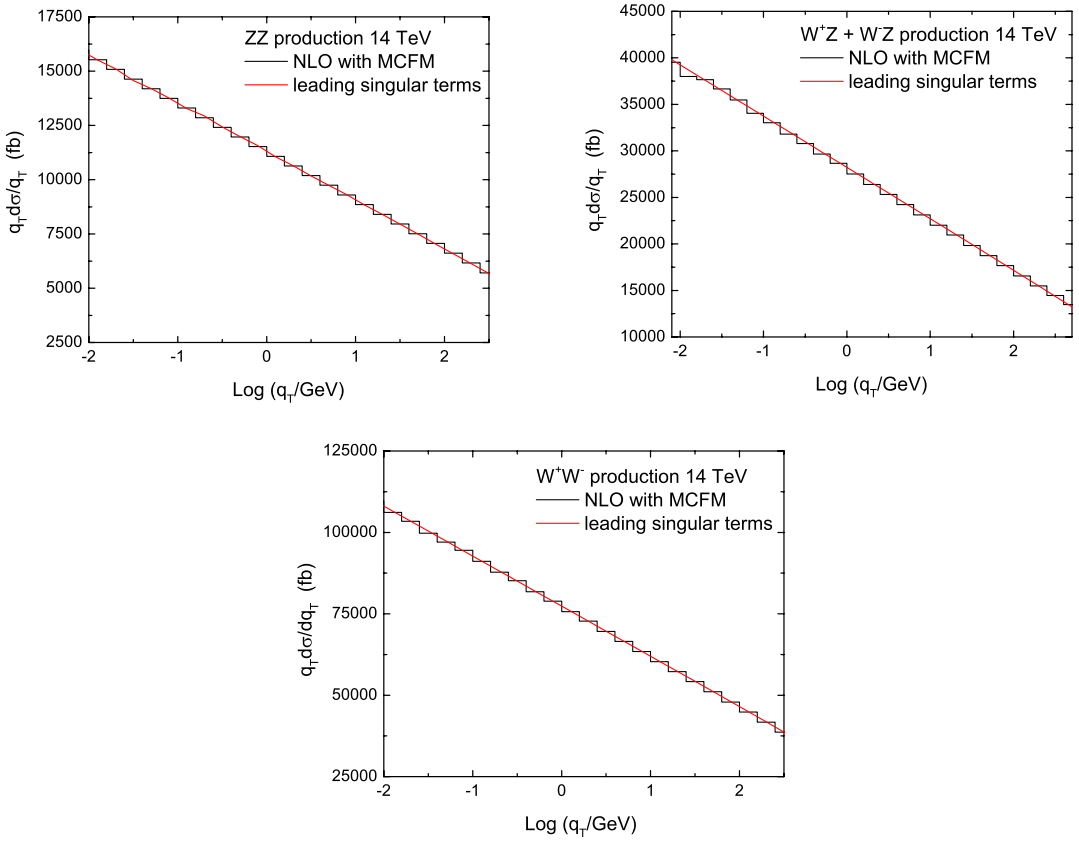

FIG. 1 (color online). Comparison of the leading singular (red) and the exact NLO (black) distributions in the small q_T region.

$$m_W = 80.4 \text{ GeV}, \quad m_Z = 91.19 \text{ GeV}, \quad \alpha(m_Z) = 1/132.338. \tag{19}$$

We use the MSTW2008NNLO PDF set and the corresponding running QCD coupling constant. The QCD coupling constant has a flavor threshold at $\mu_b = 4.75$ GeV for the b quark. The NLO QCD corrections in Eq. (18) are calculated by Monte Carlo for FeMtobarn processes (MCFM) [17]. The factorization scale is set as $\mu_f = q^* + q_T$ [33], and q^* is defined as $q^* = M\exp(-2\pi/(\Gamma_0^F \alpha_s(q^*))$, which ensures that x_T decouples from q_T^{-1} and does not contribute in the long-distance region when $q_T \to 0$. In order to contain the π^2 resummation effects to improve the perturbative convergence, we choose $\mu_h^2 = -M^2$. At NLO, we consistently choose the factorization scale and renormalization scale as M. The large logarithmic terms between hard scale and factorization scale are resumed by RG equations.

Due to the fact that the invariant mass has a minimum value for $M \geq m_{V_l} + m_{V_m} \geq 160.8$ GeV, the value of q^* has a lower limit as $q^* \geq 2.2$ GeV, and the expectation values $\langle q^* \rangle$ after the integration over invariant mass are 2.65 GeV for W^+W^-, 2.81 GeV for $W^\pm Z$, and 2.74 GeV for the ZZ process, respectively, which are larger than those in the Drell-Yan process, where $q^* = 2.04$ GeV.

A. Fixed-order results and nonperturbative effects

When resummation formula Eq. (16) is expanded to $\mathcal{O}(\alpha_s)$ in the limit $q_T \to 0$, the leading singular predictions should agree with the exact NLO results [33]. In Fig. 1, we compare the leading singular results and exact NLO results calculated by MCFM. It is shown that they are consistent with each other.

When discussing operator-product expansion of the transverse-position dependent PDFs $\mathcal{B}_{q/N}$, a hadronic form factor $f_{\text{hadr}}(x_T \Lambda_{NP})$ is introduced [33]. The form factor is used to ensure that transverse-position-dependent PDFs vanish rapidly when the transverse distance x_T is larger than the proton size,

$$\mathcal{B}_{q/N}(z, x_T^2, \mu_f) = \mathcal{B}^{\text{pert}}_{q/N}(z, x_T^2, \mu_f) f_{\text{hadr}}(x_T \Lambda_{NP}). \tag{20}$$

Here the form factor has the form

$$f_{\text{hadr}}(x_T \Lambda_{NP}) = \exp(-x_T^2 \Lambda_{NP}^2). \tag{21}$$

In Fig. 2, we present the nonperturbative effects on the differential cross sections of gauge boson pair resummation at the LHC with $\sqrt{S} = 14$ TeV. Obviously, Fig. 2 shows that the nonperturbative effects result in a tiny shift on the q_T spectrum. Since the effects are almost negligible, we choose a medium value $\Lambda_{NP} = 0.6$ GeV in the following numerical calculations without loss of generality. Once

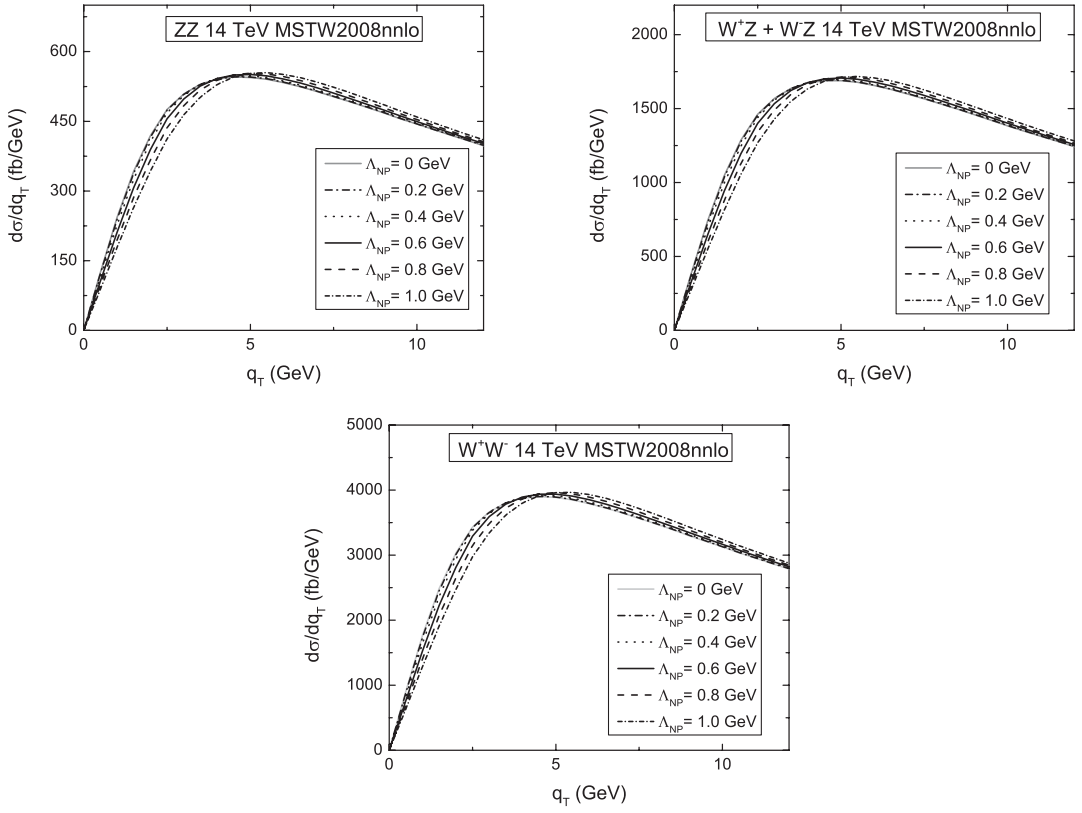

FIG. 2. The nonperturbative effects on the differential cross sections of gauge boson pair production with $\sqrt{S} = 14$ TeV, respectively.

there exist more precise experiment data, we can fit the value of Λ_{NP} by those data, and estimate the influence of nonperturbative effects.

B. Resummation results

Fig. 3 shows the resummed q_T distributions for W^+W^-, ZZ, and $W^\pm Z$ productions at next-to-leading logarithmic (NLL) and NNLL + NLO accuracy at the LHC with $\sqrt{S} =$ 8 and $\sqrt{S} = 14$ TeV, respectively, which include the uncertainties of the theoretical predictions by varying the factorization scale μ_f by a factor of two around the default choice. In these three cases of the gauge boson pair productions, the peak heights of the q_T spectrums for $\sqrt{S} =$ 14 TeV are much larger than that for $\sqrt{S} = 8$ TeV, and the peak positions have a shift of about 0.5 GeV, respectively. Besides it is shown that, compared with the NLL results, the NNLL + NLO predictions significantly reduce the scale uncertainties, which make the theoretical predictions more reliable.

We can also see that, since we consider the π^2 resummation effects, the plot displays a well convergence for W^+W^- and ZZ production. For $W^\pm Z$ production, the NNLL results are still much larger than the NLL predictions in the peak region. The difference between $W^\pm Z$ and others channels caused by the effects of the hard function for $W^\pm Z$ production, the contributions of which are much larger than those for W^+W^- and ZZ process Ref. [38].

In Fig. 3 the K factors, defined as $\sigma_{\mathrm{NNLL+NLO}}/\sigma_{\mathrm{NLO}}$, are also shown. The fixed-order predictions are calculated by MCFM and are invalid at small q_T region. In these three cases, at $q_T = 50$ GeV, the K factors are 1.7–1.8 for $\sqrt{S} =$ 8 and 1.5–1.6 for $\sqrt{S} = 14$ TeV, respectively. And in the very large q_T region, resummed results agree with MCFM predictions. Note that, to our knowledge, the q_T distribution of $W^\pm Z$ production at NNLL + NLO accuracy was not previously available in both SCET and CSS frameworks.

In Fig. 4, we show the PDF uncertainties of the NNLL order transverse-momentum distributions of the gauge boson pair at 2σ deviation for $\sqrt{S} = 14$ TeV. The PDF uncertainties are of order 5% at the low q_T region and decrease to 2.5% at the high q_T region for all three cases, respectively. We also show the PDF uncertainties with CT10NNLO PDF sets in the same plots, and the PDF uncertainties are a little larger than the cases with MSTW2008NNLO PDF sets. The situations for $\sqrt{S} = 8$ TeV are almost the same, and we do not discuss them here.

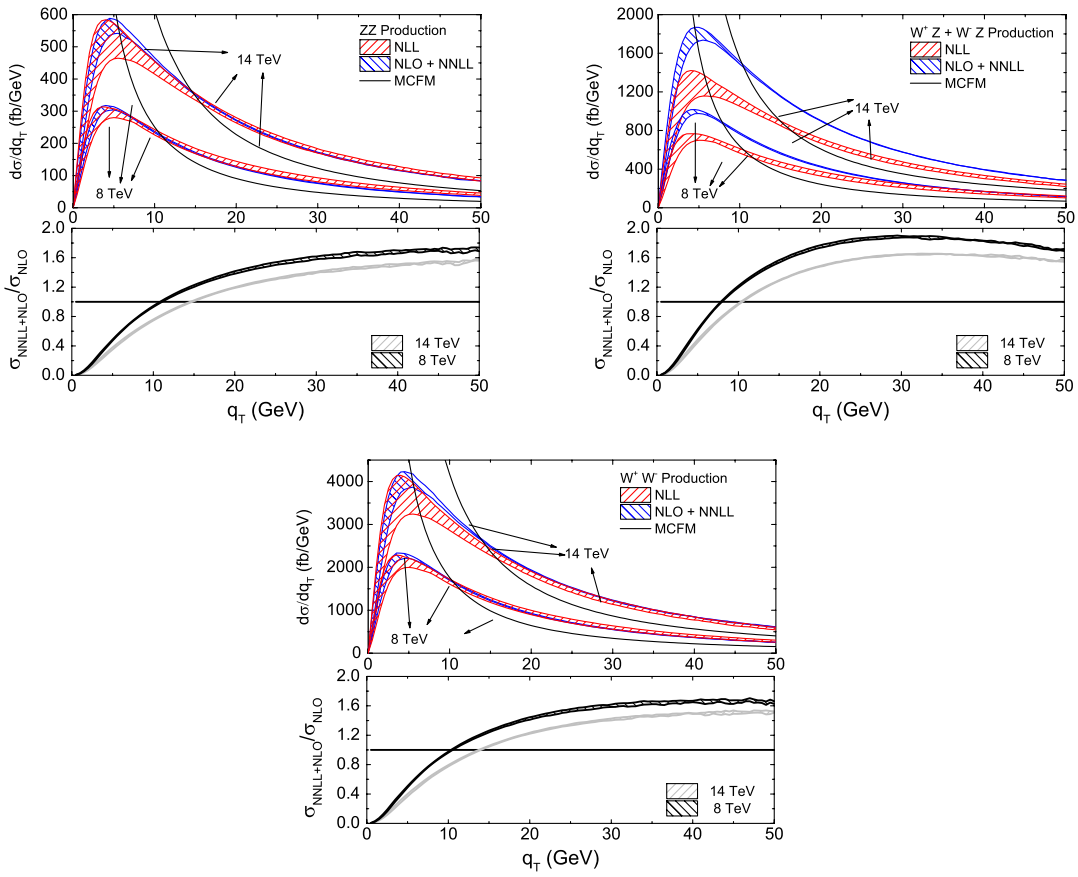

FIG. 3 (color online). Up: the q_T distributions with scale uncertainties for gauge boson pair productions at the LHC with $\sqrt{S} = 8$ and $\sqrt{S} = 14$ TeV, while the hard scale is $\mu_h^2 = -M^2$. Down: NNLL + NLO results normalized to NLO.

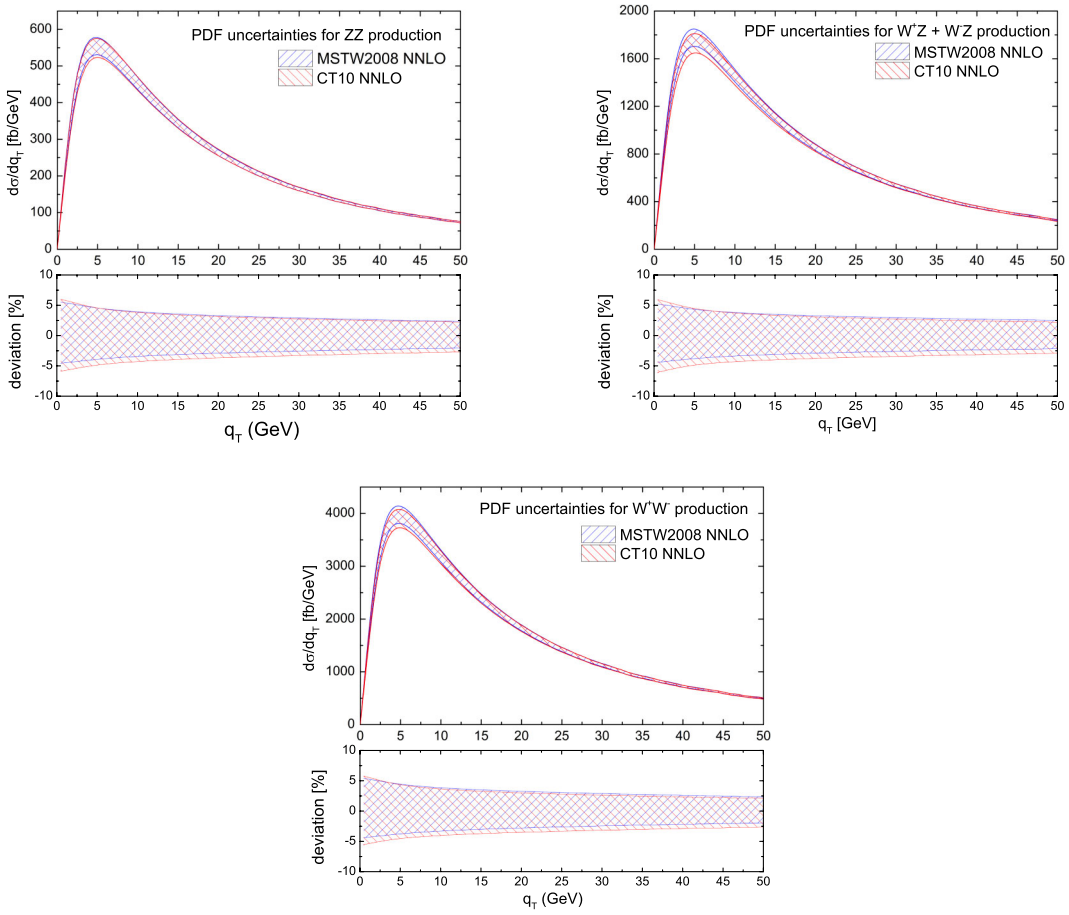

FIG. 4 (color online). The PDF uncertainties of NNLL order resummed transverse momentum for gauge boson pair production, where the bands represent 2σ deviation.

In Fig. 5, we compare our NNLL + NLO results with previous studies [34,35] in the CSS framework with MRST2002NLO PDF set for $\sqrt{S} = 14$ TeV. The peak positions of the transverse-momentum spectrum for W^+W^- and ZZ productions in our results and those in CSS results are both at about 5 GeV. However, as shown in Fig. 5, in the small q_T region, the peak heights in our results are a little lower than NLL predictions in CSS framework, while in the large q_T region, the spectrum in our results are a little higher. But the approximate NNLL predictions presented in Ref. [34] are more close to our results in the small q_T region.

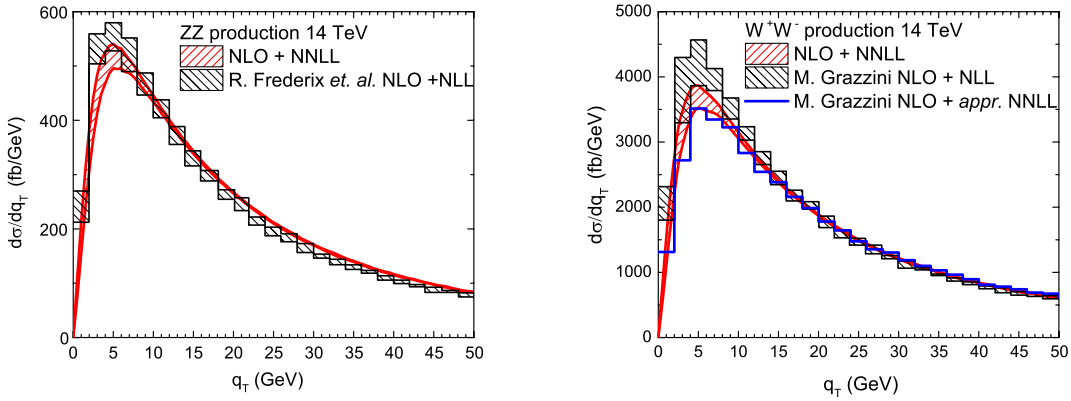

FIG. 5 (color online). Comparison of NNLL + NLO resummed q_T distribution for W^+W^- and ZZ distributions in the SCET and CSS frameworks at $\sqrt{S} = 14$ TeV with MRST2002NLO PDF set.

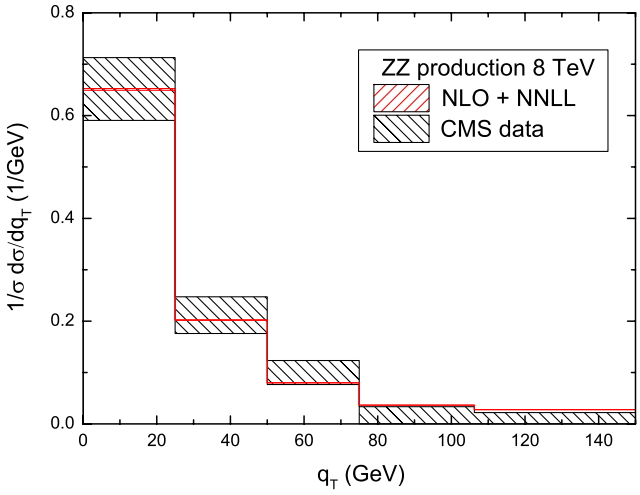

FIG. 6 (color online). Comparison of normalized q_T distribution for ZZ productions between CMS experimental data and resummation prediction at the LHC with $\sqrt{S} = 8$ TeV.

There are three possible reasons to explain the discrepancy. First, the formalism of the transverse-momentum resummation between the SCET and CSS frameworks has been compared in Ref. [32], where it shows that the lower-order anomalous dimensions are used in the NLL predictions in the CSS framework, compared with the NNLL predictions in the SCET framework. Therefore, as shown in Fig. 5, the scale uncertainties of the former (black bands) are larger than the latter (red bands). Second, the power-counting methods in two schemes are different. The third reason is probably due to the fact that the choices of scales in the two schemes are different. In the CSS framework, the renormalization and the factorization scale are set to $2m_{W/Z}$, and the resummation scale is the invariant mass of the gauge boson pair. However in the SCET framework, there are only the factorization scale and hard scale. The factorization scale is chosen as $q^* + q_T$, as described in Sec. II, while the hard scale is taken as the invariant mass of the gauge boson pair.

In Fig. 6, we compare the resummed results for the normalized differential cross section with the experimental data measured by the CMS Collaboration [12] for ZZ production at the LHC with $\sqrt{S} = 8$ TeV. Obviously, our NNLL + NLO predictions are consistent with the experimental data within theoretical and experimental uncertainties.

IV. CONCLUSION

We have studied the transverse-momentum resummation for W^+W^-, ZZ, and $W^\pm Z$ pair productions at the NNLL + NLO accuracy with SCET at the LHC. Importantly, this is the first calculation of $W^\pm Z$ transverse-momentum resummation at the NNLL + NLO accuracy. The nonperturbative effects are also included in our calculations. In these three cases of the gauge boson pair productions, our results show that the peak positions are all around 5 GeV for $\sqrt{S} = 8$ and $\sqrt{S} = 14$ TeV, respectively, which agree quite well with previous results for W^+W^- and ZZ productions, and the PDF uncertainties are less than 5% at the 2σ level for the peak region. We also find that our results agree well with experimental data reported by the CMS Collaboration for the ZZ productions at $\sqrt{S} = 8$ TeV within theoretical and experimental uncertainties.

ACKNOWLEDGMENTS

This work was supported by the National Natural Science Foundation of China, under Grants No. 11021092 and No. 11135003.

APPENDIX A: RESULTS FOR HARD FUNCTION

Here, we show the detailed results of $\mathcal{H}_{V_lV_m}(M, \mu_h)$ of the gauge boson pair production. We define

$$\mathcal{H}_{V_lV_m}(M, \mu_h) = \frac{1}{2s}\int H_{V_lV_m}(s, t, u, \mu_h)\frac{d^3p_3}{(2\pi)^3 2E_3} \times \frac{d^3p_4}{(2\pi)^3 2E_4}(2\pi)^4\delta^4(q - p_3 - p_4), \tag{A1}$$

and expand $H_{V_lV_m}$ as

$$H_{V_lV_m} = H^{(0)}_{V_lV_m} + \frac{\alpha_s}{2\pi}H^{(1)}_{V_lV_m}. \tag{A2}$$

The leading-order coefficient is

$$H^{(0)}_{V_lV_m} = \overline{|\mathcal{M}^B_{V_lV_m}|^2}, \tag{A3}$$

where $\overline{|\mathcal{M}^B_{V_lV_m}|^2}$ is the color-averaged and spin-averaged tree-level matrix element squared. $H^{(1)}_{V_lV_m}$ can be divided into two parts,

$$H^{(1)}_{V_lV_m} = \frac{\alpha_s}{2\pi}(H^{(1)}_{V_lV_m,\mathrm{reg}} + H^{(1)}_{\mu}), \tag{A4}$$

where $H^{(1)}_{\mu}$ has the same form for three cases:

$$H^{(1)}_{\mu} = C_F H^{(0)}_{V_lV_m}\left(-\ln^2\frac{M^2}{\mu_h^2} + 3\ln\frac{M^2}{\mu_h^2} - \frac{\pi^2}{6}\right). \tag{A5}$$

For simplicity, we define that all scalar one-loop integrals should be understood as retaining the finite part, and

$$\begin{aligned} \mathrm{C}_0^s &= \mathrm{C}_0(0, 0, s, 0, 0, 0), \\ \mathrm{C}_0^{V_1,V_2} &= \mathrm{C}_0(m^2_{V_1}, s, m^2_{V_2}, 0, 0, 0), \\ \mathrm{C}_0^{V,t} &= \mathrm{C}_0(0, m^2_V, t, 0, 0, 0), \\ \mathrm{D}_0^{V_1,V_2} &= \mathrm{D}_0(0, 0, m^2_{V_1}, m^2_{V_2}, s, t, 0, 0, 0, 0). \end{aligned} \tag{A6}$$

1. ZZ production

The leading-order (LO) coefficient is [15]

$$H^{(0)}_{ZZ} = \frac{1}{N_c}((g^L_{i,Z})^4 + (g^R_{i,Z})^4) \times \left(\frac{-(m_Z)^4(t^2 - 8tu + u^2) - 4tu(m_Z)^2(t+u) + tu(t^2+u^2)}{t^2u^2}\right), \tag{A7}$$

where $g^{L,R}_{i,Z}$, $i = u, d$ is the coupling between the Z boson and quarks,

$$g^L_{u,Z} = \frac{e}{\sin\theta_W\cos\theta_W}\left(\frac{1}{2} - \frac{2\sin^2\theta_W}{3}\right), \quad g^L_{d,Z} = \frac{e}{\sin\theta_W\cos\theta_W}\left(-\frac{1}{2} + \frac{\sin^2\theta_W}{3}\right), \quad g^R_{u,Z} = -\frac{2}{3}\tan\theta_W, \quad g^R_{d,Z} = -\frac{1}{3}\tan\theta_W, \tag{A8}$$

where θ_W is the Weinberg angle. The functions at the $\mathcal{O}(\alpha_s)$ are [15]

$$\frac{\alpha_s}{2\pi}H^{(1)}_{ZZ,\mathrm{reg}} = \frac{1}{12}\frac{\alpha_s}{2\pi}C_F((g^L_{i,Z})^4 + (g^R_{i,Z})^4)\Big(\mathrm{A1}(t,u) + \mathrm{A2}(t,u)\ln\left(-\frac{m_Z^2}{t}\right) + \mathrm{A3}(t,u)\ln\left(-\frac{m_Z^2}{s}\right) + \mathrm{A4}(t,u)\mathrm{D}_0^{Z,Z} + \mathrm{A5}(t,u)\mathrm{C}_0^{Z,t} + \mathrm{A6}(t,u)\mathrm{C}_0^{Z,Z} + \mathrm{A7}(t,u)\mathrm{C}_0^{s} + (t \Leftrightarrow u)\Big), \tag{A9}$$

where

$$A1(t,u) = \frac{2(m_Z^2+t)^2}{stu(1-\frac{4m_Z^2}{s})} + \frac{4s}{u(t-m_Z^2)} - \frac{-36m_Z^6 + 18m_Z^4 s + t^2(28s - 68m_Z^2) + t(88m_Z^4 - 36m_Z^2 s + 18s^2) + 16t^3}{st^2u}, \tag{A10}$$

$$A2(t,u) = -\frac{6(m_Z^4+s^2)}{stu} - \frac{4m_Z^2 s}{u(t-m_Z^2)^2} + \frac{12s}{u(t-m_Z^2)} + \frac{6m_Z^4(2m_Z^2 - s)}{st^2u} + \frac{2(4s+t)}{su}, \tag{A11}$$

$$A3(t,u) = -\frac{-12m_Z^6 + t(25m_Z^4 + 6s^2) + 6m_Z^4 s + t^2(8s - 18m_Z^2) + 5t^3}{st^2u} + \frac{-25m_Z^4 - 26m_Z^2 t + 3t^2}{stu(1-\frac{4m_Z^2}{s})} - \frac{12m_Z^2(m_Z^2+t)^2}{s^2tu(1-\frac{4m_Z^2}{s})^2}, \tag{A12}$$

$$A4(t,u) = \frac{-12m_Z^4 + 8m_Z^2 t - 2s^2 - 2t^2}{u} + \frac{4m_Z^4(2m_Z^2 - s)}{tu}, \tag{A13}$$

$$A5(t,u) = \frac{8m_Z^6(2m_Z^2 - s)}{st^2u} + \frac{4(10m_Z^4 - 5m_Z^2 t + s^2 + t^2)}{su} + \frac{4m_Z^2(-10m_Z^4 + 2m_Z^2 s - s^2)}{stu}, \tag{A14}$$

$$A6(t,u) = \frac{-3m_Z^6 + 12m_Z^4 s - 4m_Z^2 s^2 + t^2(2s - 3m_Z^2) + t(6m_Z^4 - 8m_Z^2 s) + 2s^3}{stu} + \frac{12m_Z^4(m_Z^2+t)^2}{s^2tu\left(1-\frac{4m_Z^2}{s}\right)^2} - \frac{-27m_Z^6 - 30m_Z^4 t + m_Z^2 t^2}{stu(1-\frac{4m_Z^2}{s})}, \tag{A15}$$

$$A7(t,u) = \frac{4}{3}\left(\frac{(s-2m_Z^2)^2}{stu} + \frac{-4m_Z^2 + 4s + t}{su}\right). \tag{A16}$$

2. $W^{\pm}Z$ production

The LO results can be expressed as [38]

$$H^{(0)}_{W^{\pm}Z} = \frac{1}{6}\left(\frac{1}{2\sqrt{2}\sin\theta_W}\right)^2((g^L_{d,Z})^2 I^{(0)}_{dd}(s,t,u) + 2g^L_{d,Z}g^L_{u,Z}I^{(0)}_{ud}(s,t,u) + (g^L_{u,Z})^2 I^{(0)}_{dd}(s,u,t) + 2g_{W,Z}g_{d,Z}(F^{(0)}_d(s,t,u) - F^{(0)}_d(s,u,t)) + g^2_{W,Z}J^{(0)}(s,t,u)), \tag{A17}$$

where

$$g_{W,Z} = \frac{-e}{s - m_W^2} \frac{\cos\theta_W}{\sin\theta_W}, \tag{A18}$$

and

$$I_{dd}^{(0)}(s,t,u) = 8\left(\frac{s(m_W^2+m_Z^2)}{2m_W^2m_Z^2} + \frac{1}{4}\left(\frac{tu}{m_W^2m_Z^2} - 1\right)\right) + 8\left(\frac{u}{t} - \frac{m_W^2m_Z^2}{t^2}\right), \tag{A19}$$

$$I_{ud}^{(0)}(s,t,u) = \frac{8s(m_W^2+m_Z^2)}{tu} - 8\left(\frac{s(m_W^2+m_Z^2)}{2m_W^2m_Z^2} + \frac{1}{4}\left(\frac{tu}{m_W^2m_Z^2} - 1\right)\right), \tag{A20}$$

$$F_d^{(0)}(s,t,u) = -8s\left(\frac{1}{4}\left(-\frac{4m_W^2m_Z^2}{st} - \frac{m_W^2+m_Z^2}{s} + 1\right)\left(\frac{tu}{m_W^2m_Z^2} - 1\right) + \frac{(m_W^2+m_Z^2)\left(\frac{2m_W^2m_Z^2}{t} - m_W^2 - m_Z^2 + s\right)}{2m_W^2m_Z^2}\right), \tag{A21}$$

$$J^{(0)}(s,t,u) = 8s^2\left(\frac{8m_W^2m_Z^2 + (m_W^2+m_Z^2)^2}{4s^2} - \frac{m_W^2+m_Z^2}{2s} + \frac{1}{4}\right)\left(\frac{tu}{m_W^2m_Z^2} - 1\right) + \frac{8s^2(m_W^2+m_Z^2)\left(\frac{(m_W^2-m_Z^2)^2}{2s} - m_W^2 - m_Z^2 + \frac{s}{2}\right)}{m_W^2m_Z^2}. \tag{A22}$$

When considering virtual corrections, as in the tree-level case, we have [38]

$$\begin{aligned}\frac{\alpha_s}{2\pi}H_{W^\pm Z,\mathrm{reg}}^{(1)} = \frac{1}{6}\frac{\alpha_s}{2\pi}C_F\left(\frac{1}{2\sqrt{2}\sin\theta_W}\right)^2\big((g_{d,Z}^L)^2 I_{dd}^{(1)}(s,t,u) + g_{d,Z}^L g_{u,Z}^L I_{ud}^{(1)}(s,t,u) + (g_{u,Z}^L)^2 I_{dd}^{(1)}(s,u,t) \\ + g_{W,Z}g_{d,Z}(F_d^{(1)}(s,t,u) - F_d^{(1)}(s,u,t)) + g_{W,Z}^2 J^{(1)}(s,t,u)\big),\end{aligned} \tag{A23}$$

where

$$\begin{aligned}I_{dd}^{(1)} = {} & \frac{2(22t^2 + t(19s - 18\Sigma) + 18m_W^2m_Z^2)}{t^2} - \frac{8(ut + 2s\Sigma)}{m_W^2m_Z^2} - \frac{2(t-u)^2}{ts\beta^2} \\ & + \left(\frac{2(8t^2 + 4t(s-3\Sigma) + 4\Sigma^2 - 5s\Sigma + s^2)}{ts\beta^2} + \frac{4(t(3u+s) - 3m_W^2m_Z^2)}{t^2} + \frac{6(t+u)(t-u)^2}{ts^2\beta^4}\right)\ln\left(-\frac{t}{s}\right) \\ & + \left(\frac{8t^2(-2s+\Delta) + 8t(-s^2 + 3s\Sigma - 2\Delta\Sigma) - 2(s-\Sigma)(s^2 - 4s\Sigma + 3\Delta\Sigma)}{ts^2\beta^2} + \frac{16s(t - m_Z^2)}{t(u+s) - m_W^2m_Z^2}\right. \\ & \left. - \frac{6(s-\Delta)(t+u)(t-u)^2}{ts^3\beta^4} + \frac{2(4t^2 + t(10s - 3m_Z^2 - 9m_W^2) + 12m_W^2m_Z^2)}{t^2}\right)\ln\left(-\frac{t}{m_W^2}\right) \\ & + \left(-\frac{4t^2(2\Sigma - 3s) - 4t(s-\Sigma)(2s - 3\Sigma) - 2(s-2\Sigma)(s-\Sigma)^2}{ts\beta^2}\right. \\ & \left. + \frac{4\Sigma t - 3s^2 + 4s\Sigma - 4(m_W^4 + m_Z^4)}{t} - \frac{3(t^2-u^2)^2}{ts^2\beta^4}\right)\mathrm{C}_0^{W,Z} \\ & + \left(\frac{4(ut + 2s\Sigma)}{3m_W^2m_Z^2} - \frac{4(t-2u)}{3t}\right)\mathrm{C}_0^s - \frac{4s(tu - 2m_W^2m_Z^2)\mathrm{D}_0^{W,Z}}{t} \\ & + \frac{(8(t - m_W^2)(ut - 2m_W^2m_Z^2))\mathrm{C}_0^{W,t}}{t^2} + (m_W \Leftrightarrow m_Z),\end{aligned} \tag{A24}$$

$$
\begin{aligned}
I_{ud}^{(1)} = {} & \frac{4s^2(2t-\Sigma)}{u(m_W^2 m_Z^2 - t(s+u))} + \frac{8(2s\Sigma + tu)}{m_W^2 m_Z^2} + \frac{2(-18s\Sigma + t(9s-4\Sigma) + 4t^2)}{tu} \\
& + \left(\frac{2(-(s-\Sigma)(3s+4\Sigma) - 4t(s+3\Sigma) + 8t^2)}{\beta^2 su} + \frac{6(t+u)(t-u)^2}{\beta^4 s^2 u} - \frac{12s(t-\Sigma)}{tu}\right)\ln\left(-\frac{t}{s}\right) \\
& + \left(\frac{2}{us^2\beta^2}(4t^2(-2s+\Delta) + 4t(s^2 + s(m_Z^2 + 5m_W^2) - 2\Delta\Sigma) + (s-\Sigma)(3s^2 + 8sm_W^2 - 3\Delta\Sigma)) \right. \\
& - \frac{8s^2 t(t-m_Z^2)(2t-\Sigma)}{u(m_W^2 m_Z^2 - t(s+u))^2} + \frac{2t(2m_W^2 + m_Z^2 + 18s) - 24s\Sigma}{tu} + \frac{6(s-\Delta)(s-\Sigma)(t-u)^2}{\beta^4 s^3 u} \\
& \left. - \frac{8s(-t(2m_W^2 + 4m_Z^2 + 3s) + 2m_Z^2(s+\Sigma) + 2t^2)}{u(m_W^2 m_Z^2 - t(s+u))}\right)\ln\left(-\frac{t}{m_W^2}\right) \\
& + \left(-\frac{2((s-\Sigma)^2(s+2\Sigma) + 2t^2(2\Sigma - 3s) + 6\Sigma t(s-\Sigma))}{\beta^2 su} + \frac{3s(-s-4\Sigma+4t)}{u} - \frac{3(s-\Sigma)^2(t-u)^2}{\beta^4 s^2 u}\right)\mathrm{C}_0^{W,Z} \\
& + \frac{8s^2(t-\Sigma)}{u}\,\mathrm{D}_0^{W,Z} + \left(\frac{4(4s+u)}{3u} - \frac{4(2s\Sigma+tu)}{3m_W^2 m_Z^2}\right)\mathrm{C}_0^{s} - \frac{16s(t-m_W^2)(t-\Sigma)}{tu}\,\mathrm{C}_0^{W,t} \\
& + (t \Leftrightarrow u) + (m_W \Leftrightarrow m_Z) + (t \Leftrightarrow u, m_W \Leftrightarrow m_Z),
\end{aligned} \tag{A25}
$$

$$
\begin{aligned}
F_d^{(1)} = {} & \frac{4(17(m_W^2 m_Z^2 + s\Sigma) + t(11s - 13\Sigma) + 17t^2)}{t} + \frac{16(s-\Sigma)(2s\Sigma+tu)}{m_W^2 m_Z^2} + \frac{4s^2(2t-\Sigma)}{t(s+u) - m_W^2 m_Z^2} \\
& + \left(\frac{8(t-u)}{\beta^2} - \frac{4(3(m_W^2 m_Z^2 + s\Sigma) - t(s+3\Sigma) + 3t^2)}{t^2}\right)\ln\left(-\frac{t}{s}\right) \\
& + \left(\frac{8(3(m_W^2 m_Z^2 + s\Sigma) - t(3m_W^2 + m_Z^2 + 2s) + t^2)}{t} + \frac{8s(t(3s+2\Sigma) - 2m_Z^2(s+\Sigma))}{t(s+u) - m_W^2 m_Z^2} + \frac{8s^2 t(t-m_Z^2)(2t-\Sigma)}{(t(s+u) - m_W^2 m_Z^2)^2} \right. \\
& \left. - \frac{8(s-\Delta)(t-u)}{\beta^2 s}\right)\ln\left(-\frac{t}{m_W^2}\right) + \left(4(-m_W^4 - m_Z^4 + 4s\Sigma) + 4t(\Sigma - 3s) + \frac{4(s-\Sigma)(t-u)}{\beta^2}\right)\mathrm{C}_0^{W,Z} \\
& - \left(\frac{8(2(m_W^2 m_Z^2 + s\Sigma) + 2t(2s-\Sigma) + 3t^2)}{3t} + \frac{8(s-\Sigma)(2s\Sigma+tu)}{3m_W^2 m_Z^2}\right)\mathrm{C}_0^{s} + 4(2s(m_W^2 m_Z^2 + s\Sigma) + st^2 \\
& - st(s+\Sigma))\mathrm{D}_0^{W,Z} - \frac{8(t-m_W^2)(2(m_W^2 m_Z^2 + s\Sigma) - t(s+\Sigma) + t^2)}{t}\,\mathrm{C}_0^{W,t} + (m_W \Leftrightarrow m_Z),
\end{aligned} \tag{A26}
$$

$$
J^{(1)} = \left(16 - \frac{8\pi^2}{3}\right)\left(m_W^4 - \frac{(s-\Sigma)^2(2s\Sigma+tu)}{m_W^2 m_Z^2} + 10m_W^2 m_Z^2 + m_Z^4 + s^2 + 6s\Sigma + 8t(s-\Sigma) + 8t^2\right), \tag{A27}
$$

with

$$
\Sigma = m_Z^2 + m_W^2, \qquad \Delta = m_Z^2 - m_W^2, \qquad \beta = \sqrt{1 - \frac{(m_W+m_Z)^2}{s}}\sqrt{1 - \frac{(m_W-m_Z)^2}{s}}. \tag{A28}
$$

3. W^+W^- production

The LO results are [13]

$$
H_{WW}^{(0)} = \frac{1}{12}(c_q^{tt} F_q^0(s,t) + c_q^{ss} K_q^0(s,t) - c_q^{ts} J_q^0(s,t)). \tag{A29}
$$

The coefficients are

$$
\begin{aligned}
c_q^{tt} &= \frac{\pi^2\alpha^2}{\sin^2\theta_W}, \qquad c_q^{ts}(s) = \frac{4\pi^2\alpha^2}{\sin^2\theta_W}\,\frac{1}{s}\left(Q_q + \frac{s}{s-m_Z^2}\,\frac{1}{\sin^2\theta_W}(T_{3,q} - Q_q\sin^2\theta_W)\right), \\
c_q^{ss}(s) &= \frac{16\pi^2\alpha^2}{s^2}\left\{\left(Q_q + \frac{1}{2\sin^2\theta_W}(T_{3,q} - 2Q_q\sin^2\theta_W)\,\frac{s}{s-m_Z^2}\right)^2 + \left(\frac{T_{3,q}}{2\sin^2\theta_W}\,\frac{s}{s-m_Z^2}\right)^2\right\},
\end{aligned} \tag{A30}
$$

with $T_{3,q} = \pm\frac{1}{2}$. The functions occurring in the lowest-order amplitudes are

$$\begin{aligned} F_u^0(s,t) &= F_d^0(s,u) = 16\left(\frac{ut}{m_W^4} - 1\right)\left(\frac{1}{4} + \frac{m_W^4}{t^2}\right) + 16\frac{s}{m_W^2}, \\ J_u^0(s,t) &= -J_d^0(s,u) = 16\left(\frac{ut}{m_W^4} - 1\right)\left(\frac{s}{4} - \frac{m_W^2}{2} - \frac{m_W^4}{t}\right) + 16s\left(\frac{s}{m_W^2} - 2 + \frac{2m_W^2}{t}\right), \\ K_u^0(s,t) &= K_d^0(s,u) = 8\left(\frac{ut}{m_W^4} - 1\right)\left(\frac{s^2}{4} - sm_W^2 + 3m_W^4\right) + 8s^2\left(\frac{s}{m_W^2} - 4\right). \end{aligned} \tag{A31}$$

The functions at the $\mathcal{O}(\alpha_s)$ are [13]

$$\frac{\alpha_s}{2\pi} H_{WW,\mathrm{reg}}^{(1)} = \frac{1}{24}\frac{\alpha_s}{2\pi} C_F (c_q^{tt} F_q^1(s,t) + c_q^{ss} K_q^1(s,t) - c_q^{ts} J_q^1(s,t)), \tag{A32}$$

where

$$\begin{aligned} F_u^1(s,t) = {} & \frac{4(80t^2 + 73st - 140m_W^2 t + 72m_W^4)}{t^2} - \frac{4(4t+s)^2}{s\beta^2 t} - \frac{128(t+2s)}{m_W^2} + \frac{64(t+s)}{m_W^4} - \left(\frac{32(t^2 - 3st - 3m_W^4)}{t^2}\right. \\ & \left. + \frac{128s}{t - m_W^2}\right)\ln\left(\frac{-t}{m_W^2}\right) + \left(\frac{8(6t^2 + 8st - 19m_W^2 t + 12m_W^4)}{t^2} - \frac{32t^2 - 128st - 26s^2}{s\beta^2 t} + \frac{6(4t+s)^2}{s\beta^4 t}\right)\ln\left(\frac{s}{m_W^2}\right) \\ & + 32s\left(\frac{2m_W^4}{t} - u\right)\mathrm{D}_0^{W,W} - 64(t - m_W^2)\left(\frac{2m_W^4}{t^2} - \frac{u}{t}\right)\mathrm{C}_0^{W,t} + \left(\frac{16t(4m_W^2 - u) - 49s^2 + 72m_W^2 s - 48m_W^4}{2t}\right. \\ & \left. + \frac{2(8t^2 - 14st - 3s^2)}{\beta^2 t} - \frac{3(4t+s)^2}{2\beta^4 t}\right)\mathrm{C}_0^{W,W} + \frac{32\pi^2}{3}\left(\frac{2(t+2s)}{m_W^2} - \frac{3t + 2s - 4m_W^2}{t} - \frac{t(t+s)}{m_W^4}\right), \end{aligned} \tag{A33}$$

$$\begin{aligned} J_u^1(s,t) = {} & -\frac{128(t^2 + 2st + 2s^2)}{m_W^2} - \frac{16(t^2 - 21st - 26m_W^2 t + 34m_W^2 s + 17m_W^4)}{t} + \frac{64st(t+s)}{m_W^4} + \frac{32s^2}{t - m_W^2} \\ & + \left(16(t - 5s + 2m_W^2) - \frac{48m_W^2(2s + m_W^2)}{t} + \frac{64s(2t+s)}{t - m_W^2} - \frac{32s^2 t}{(t - m_W^2)^2}\right)\ln\left(\frac{-t}{m_W^2}\right) \\ & + \left(\frac{16(4t+s)}{\beta^2} - 16(3t - 2s) + \frac{48m_W^2(2t - 2s - m_W^2)}{t}\right)\ln\left(\frac{s}{m_W^2}\right) + 16s(t(2s+u) - 2m_W^2(2s + m_W^2))\mathrm{D}_0^{W,W} \\ & + 32(t - m_W^2)\left(\frac{2m_W^2(2s + m_W^2)}{t} - 2s - u\right)\mathrm{C}_0^{W,t} + \left(32st - 12s^2 + 32m_W^4 - 16m_W^2(2t + 7s) - \frac{4s(4t+s)}{\beta^2}\right)\mathrm{C}_0^{W,W} \\ & + \frac{32\pi^2}{3}\left(\frac{2(t^2 + 2st + 2s^2)}{m_W^2} - \frac{st(t+s)}{m_W^4} - \frac{2m_W^2(2t - 2s - m_W^2)}{t} - t - 4s\right), \end{aligned} \tag{A34}$$

$$K_u^1(s,t) = 16\left\{12t^2 + 20st - 24m_W^2 t + 17s^2 - 4m_W^2 s + 12m_W^4 + \frac{s^2 t(t+s)}{m_W^4} - \frac{2s(2t^2 + 3st + 2s^2)}{m_W^2}\right\}\left(2 - \frac{\pi^2}{3}\right), \tag{A35}$$

with $F_d^1(s,t) = F_u^1(s,u)$, $J_d^1(s,t) = -J_u^2(s,u)$, and $K_d^1(s,t) = K_u^1(s,u)$.

[1] T. Aaltonen *et al.* (CDF Collaboration), Phys. Rev. Lett. **104**, 201801 (2010).
[2] T. Aaltonen *et al.* (CDF Collaboration), Phys. Rev. Lett. **108**, 101801 (2012).
[3] V. M. Abazov *et al.* (D0 Collaboration), Phys. Rev. D **88**, 012005 (2013).
[4] V. M. Abazov *et al.* (D0 Collaboration), Phys. Rev. D **85**, 112005 (2012).
[5] V. M. Abazov *et al.* (D0 Collaboration), Phys. Rev. D **88**, 032008 (2013).
[6] G. Aad *et al.* (ATLAS Collaboration), Phys. Rev. Lett. **108**, 041804 (2012).

[7] S. Chatrchyan *et al.* (CMS Collaboration), J. High Energy Phys. 01 (2013) 063.
[8] G. Aad *et al.* (ATLAS Collaboration), Phys. Rev. Lett. **107**, 041802 (2011).
[9] G. Aad *et al.* (ATLAS Collaboration), Eur. Phys. J. C **72**, 2173 (2012).
[10] G. Aad *et al.* (ATLAS Collaboration), Phys. Lett. B **709**, 341 (2012).
[11] G. Aad *et al.* (ATLAS Collaboration), Phys. Rev. D **87**, 112001 (2013).
[12] Report No. CMS-PAS-SMP-13-005, CERN, Geneva, 2013.
[13] S. Frixione, Nucl. Phys. **B410**, 280 (1993).
[14] J. Ohnemus and J. F. Owens, Phys. Rev. D **43**, 3626 (1991).
[15] B. Mele, P. Nason, and G. Ridolfi, Nucl. Phys. **B357**, 409 (1991).
[16] L. Dixon, Z. Kunszt, and A. Signer, Phys. Rev. D **60**, 114037 (1999).
[17] J. M. Campbell and R. K. Ellis, Phys. Rev. D **60**, 113006 (1999).
[18] L. Dixon, Z. Kunszt, and A. Signer, Nucl. Phys. **B531**, 3 (1998).
[19] G. Chachamis, M. Czakon, and D. Eiras, J. High Energy Phys. 12 (2008) 003.
[20] S. Dawson, I. M. Lewis, and M. Zeng, Phys. Rev. D **88**, 054028 (2013).
[21] F. Campanario and S. Sapeta, Phys. Lett. B **718**, 100 (2012).
[22] C. W. Bauer, S. Fleming, D. Pirjol, and I. W. Stewart, Phys. Rev. D **63**, 114020 (2001).
[23] C. W. Bauer, D. Pirjol, and I. W. Stewart, Phys. Rev. D **65**, 054022 (2002).
[24] M. Beneke, A. Chapovsky, M. Diehl, and T. Feldmann, Nucl. Phys. **B643**, 431 (2002).
[25] Y. Gao, C. S. Li, and J. J. Liu, Phys. Rev. D **72**, 114020 (2005).
[26] A. Idilbi, X.-d. Ji, and F. Yuan, Phys. Lett. B **625**, 253 (2005).
[27] T. Becher and M. Neubert, Eur. Phys. J. C **71**, 1665 (2011).
[28] T. Becher, M. Neubert, and D. Wilhelm, J. High Energy Phys. 02 (2012) 124.
[29] M. G. Echevarria, A. Idilbi, and I. Scimemi, J. High Energy Phys. 07 (2012) 002.
[30] J.-Y. Chiu, A. Jain, D. Neill, and I. Z. Rothstein, J. High Energy Phys. 05 (2012) 084.
[31] T. Becher, M. Neubert, and D. Wilhelm, J. High Energy Phys. 05 (2013) 110.
[32] T. Becher and M. Neubert, Eur. Phys. J. C **71**, 1665 (2011).
[33] T. Becher, M. Neubert, and D. Wilhelm, J. High Energy Phys. 02 (2012) 124.
[34] M. Grazzini, J. High Energy Phys. 01 (2006) 095.
[35] R. Frederix and M. Grazzini, Phys. Lett. B **662**, 353 (2008).
[36] C. Balázs and C.-P. Yuan, Phys. Rev. D **59**, 114007 (1999).
[37] H. T. Li, C. S. Li, D. Y. Shao, L. L. Yang, and H. X. Zhu, Phys. Rev. D **88**, 074004 (2013).
[38] S. Frixione, P. Nason, and G. Ridolfi, Nucl. Phys. **B383**, 3 (1992).
[39] T. Becher, M. Neubert, and G. Xu, J. High Energy Phys. 07 (2008) 030.
[40] V. Ahrens, T. Becher, M. Neubert, and L. L. Yang, Phys. Rev. D **79**, 033013 (2009).
[41] T. Becher and G. Bell, Phys. Lett. B **713**, 41 (2012).
[42] J. Beringer *et al.* (Particle Data Group), Phys. Rev. D **86**, 010001 (2012).